steel research international
www.steel-research.de

Effect of Sample Geometry on Strain Uniformity and Double Hit Compression Tests for Softening Kinetics Determination

Nusrat Tamanna, Carl Slater, and Claire Davis*

Static softening is an essential process during the hot rolling of steel to refine grain size and improve mechanical properties. The double hit test is used to measure the static softening volume fraction from the flow stress curves. Herein, the influence of different sample geometries on the determination of softening fraction from the double hit test for conditions where 0–99% softening is expected. The double hit tests are modeled in DEFORM for conventional sample geometries in both uniaxial compression and standard plane strain compression tests, and an additional simulation of a modified plane strain compression test sample geometry, designed to provide more uniform strain distributions, is also performed. A user routine is incorporated into the model to predict the localized softening volume fraction from localized strain based on known softening equations and set back the localized strain value to zero while the softening volume fraction reaches 85%. The standard plane strain compression test geometry shows a strong strain gradient resulting in inaccurate softening fraction volume predictions from flow stress, whereas the uniaxial compression test and modified plane strain compression test geometries show better predictions of softening volume fraction from the flow stress data.

1. Introduction

Thermomechanically controlled rolling is an important microstructure control process used in the steel industry to refine grain sizes via softening control which gives improved strength and toughness.[1–4] This led to widespread use of laboratory-based thermomechanical simulators, such as Gleeble and ServoTest machines, to reproduce the strain, strain rate, and temperatures of hot deformation, allowing softening behavior to be studied for different steels and supporting the optimization of rolling schedules to achieve improved microstructures and properties.[5–7] These machines use compression and torsion samples to investigate the key fundamental metallurgical processes such as softening, which is not economically viable on full-scale plant trials.[8,9]

Static softening occurs during hot rolling of steel and several methods are used to determine the softening fraction for a given strain, deformation temperature, and interpass time (time between two deformation strains).[10–12] Double hit test is a widely used approach to measure softening fraction using laboratory-based thermomechanical simulators.[13] In this test, the fraction of static softening is defined by the degree of softening after an initial deformation by carrying out a second deformation after a specified time interval.[11,14] The fraction of static softening is defined as[11]

$$X = \frac{\sigma_m - \sigma_2}{\sigma_m - \sigma_1} \quad (1)$$

where σ_1 is the flow stress at the proportional limit of the linear elastic region (i.e., yield stress) for the first deformation hit, σ_m is the peak stress in the first deformation hit, and σ_2 is the new yield stress for the second deformation hit.

To determine the flow stresses from double hit deformation, uniaxial compression tests (UCT) or plane strain compression tests (PSCT) are commonly used.[15–17] The higher the softening fraction, the lower the second deformation hit yields stress. The measured softening fraction from this equation for a specific strain, interpass time, and temperature will be dependent on the uniformity of strain in the sample and it has been reported that these test methods and standard sample geometries suffer from strain gradients. For example due to friction between the samples and anvils,[18–20] the resulting barreling effect from friction results in dead zones at the either end of the samples and a high strain concentration in the center, for example, Chamanfar et al. reported the inhomogeneity in strain distribution in uniaxial compression test cylindrical specimens of 15 mm height and 10 mm diameter.[18] Due to barreling, dead zones with average 0.63 strain formed at the top and bottom of the sample for an applied macroscopic strain of 0.83, while the center of the sample experienced ≈ 1.3 strain and the largest strain (≈ 2.5) was observed at the edge of the sample. The nonuniformity of strain distribution in plane strain samples has been reported by Mirza et al. due to thickness of sample geometry, friction coefficient,

N. Tamanna, C. Slater, C. Davis
Warwick Manufacturing Group
University of Warwick
Coventry CV4 7AL, UK
E-mail: Nusrat.Tamanna@warwick.ac.uk

The ORCID identification number(s) for the author(s) of this article can be found under https://doi.org/10.1002/srin.202200157.

DOI: 10.1002/srin.202200157

and strain rate.[21] The range of strain distribution of the deformed area varied from 0.25 to 1.79 for 50% reduction. The change of deformation zone shape was observed for different thicknesses of the samples, for example, the deformation zone shape changes from a double "X" shape to a "V" shape for workpiece thicknesses of 0.58–0.66 mm.[17] The plastic strain distribution was heterogeneous, varying in the range 0.15–0.28 for applied 0.22 strain. The authors previous work has shown that there is strong inhomogeneity in the strain distribution in UCT samples and in the standard PSCT sample using a 10 mm-wide anvil.[22] A modified PSCT has been proposed that uses 20 mm-wide anvils to ensure that the shear strains generated at the edges of the anvils do not interact at the core of the sample and this geometry provides much greater strain uniformity and a large area corresponding to the applied macroscopic strain that is suitable for microstructural assessment to determine the recrystallized grain size distributions.[22] The effect of strain inhomogeneity on the flow stress behavior during double hit tests used to determine the softening volume fraction has not been reported for the different sample geometries.

In this work, UCT, standard PSCT, and modified PSCT samples were used to see the effect of different geometries on strain uniformity and its subsequent effect on the prediction of softening fraction from double hit flow stress. 3D finite element modelling (FEM) double hit test models were developed using DEFORM software to predict flow stress. To develop double hit test models, a Fortran-based user routine was used and coupled with DEFORM to calculate the localized softening fraction from the localized strain and set back the localized strain value to zero once the localized softening fraction reached 85%. The flow stresses from the double hit tests model were used to predict total softening of the samples using the 0.2% offset method. The strong strain gradient in standard PSCT causes more deviation from the applied softening fraction condition based on empirical conditions. The predicted flow stress and softening fraction from flow stress of three geometries was validated experimentally.

2. Methodology

2.1. Materials and Softening Kinetics

In this work, C–Mn steel with known softening kinetics was used to see the effect of different geometries on the measurement of softening fraction from double hit tests. To develop empirical equations (Equation (2) and (3)) of softening fraction and the starting time of the C–Mn steel, PSCT2 samples were deformed in the Gleeble to 0.3 strain and held for varying temperatures and holding times. Then samples were analyzed in scanning electron microscope (SEM) to take electron backscatter diffraction (EBSD) images. From the EBSD microstructure, softening fraction for each experiment was calculated and fit with the equation to calculate materials properties and activation energy of softening kinetics. The softening starting time and softening fraction volume equations of the current C–Mn steel are given in Equation (2) and (3).

$$R_s = A_3 \varepsilon^{-4} D_o^2 \exp\left(\frac{Q}{RT}\right) \quad (2)$$

$$X_{srex} = 1 - \exp\left[\beta_s \times \frac{t}{R_s}\right]^{k_s} \quad (3)$$

where R_s, A_3, ε, D_o, Q, and T are the softening starting time, material constant (8.68e–20), strain (0.3), initial austenite grain size (185 μm), activation energy of softening (311 826 J mol^{-1}), and temperature, respectively. X_{srex} is the softening fraction. β_s and k_s the material-dependent constants with values of LN(0.95) and 2, respectively.

Based on empirical equations (from Equation (2) and (3)), we calculated interpass time between double hit to achieve 0%, 25%, 50%, 75%, and 99% static softening fractions for a specific temperature (1000 °C) and macroscopically uniform strain (0.3). From literature, it is observed that 0.3 strain is used to analyze static softening for C–Mn steel at 1000 °C.[23] Therefore the first hit for all experiments and models was performed up to 0.3 strain. For the used material significant grain growth has been determined not to occur until the temperature is >1000 °C and interpass time longer than 1 min.[24]

2.2. Finite-Element modeling

Deform v12.0.1 software was used to develop a 3D model for UCT and PSCT. In UCT, cylindrical specimens of 15 mm height and 10 mm diameter were used. For both PSCT1 and PSCT2, the same sample size (10 mm height, 20 mm width, and 50 mm length) was used, but for PSCT2 a wider anvil is used which improves the uniformity of strain distribution.[22] The three samples and anvil geometries are summarized in **Table 1**.

DEFORM models were used to predict the local strain distribution in the sample, and a user routine in FORTRAN was written to determine the local softening behavior from local strain (based on the strain, temperature, interpass time, and known material softening behavior). The local strain value after each time step was used as input into the user routine and when the local mesh element conditions reached 85% softening, the strain was forced to return zero before the second deformation hit.

A macroscopic strain of 0.3 was applied at a strain rate of 1 s^{-1} for both deformation hits. The samples and anvils were considered plastic and rigid bodies, respectively. A friction coefficient of 0.15 was used between the sample and anvil based on that previously used in the literature and the observed barreling effect after deformation[6] and verified by comparing the spread of width between model and experimental samples after deformation. All double hit tests were performed considering a uniform temperature of 1000 °C for different holding times (interpass times). After double hit tests, load and displacement were extracted from the models to calculate flow stress.

The interpass times between the two deformations were selected for 0%, 25%, 50%, 75%, and 99% softening fractions

Table 1. Summary of compression test simulations.

Sample	Sample geometry	Anvil geometry
UCT	Cylinder 10 mm Ø × 15 mm length	30 mm Ø
PSCT1	10 × 20 × 50 mm (H × W × L)	10 × 80 mm
PSCT2	10 × 20 × 50 mm (H × W × L)	20 × 80 mm

based on the empirical equation of softening kinetics (from Equation (2) and (3)) and applied 0.3 macroscopic strain at 1000 °C. Though softening of metal involves both recovery and softening, recovery was not accounted for in the model. As the conditions for deformation were the same for all geometry types, recovery would be the same in all cases.

2.3. Method of Simulating Softening Fraction from Double Hit Test

During a double hit test, an initial strain was applied to the specimen during the first deformation hit. After the first deformation hit, the sample was held for a specific time (interpass time) at the deformation temperature to allow static softening to occur. The static softening fraction depends on the deformation temperature, applied initial strain, and inter-pass time. Finally, a second deformation hit was performed for a specific strain.

Figure 1 gives an example of the double hit test flow stress–strain data from the FE model. The first deformation hit was performed at 1000 °C, at a strain rate of $1\,s^{-1}$ and up to 0.3 strain, and then an inter-pass time of 15 s was applied in the model. For this interpass time, 56% static softening was predicted from the flow stress.

The stress-strain curves were simulated to determine peak stress and yield stresses to calculate softening fraction volume from Equation (1) where interpass times between deformations were selected for 0%, 25%, 50%, 75%, and 99% softening fractions from empirical equations (from Equation (2) and (3)) for applied 0.3 macroscopic strain. The input initial grain size in the model was used from the experimental data to keep the similarity between the model and experiment. To measure the initial grain size, samples were heated up to 1200 °C for 5 min to austenitize and then quenched. Then samples were analyzed in scanning electron microscope (SEM) to measure the average grain size.

The yield stress of the second deformation was equal to the flow stress at the end of the first deformation when the interpass time was zero. When the interpass time was increased, the yield stress during the second deformation hit was reduced as static softening occurred, when 99% softening occurred, the yield stresses from the first and second deformation were approximately the same (minor difference due to grain size difference effect). The yield stress was calculated based on the 0.2% offset method.

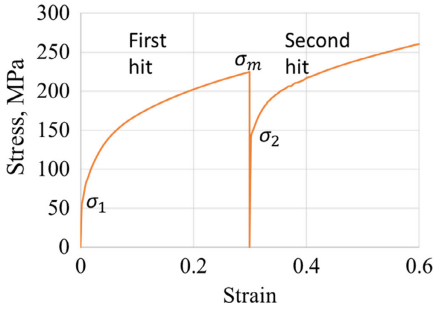

Figure 1. Calculation of softening fraction from double hit test.

2.4. Model Verification

To verify the double hit test models, all samples were deformed in a Gleeble HDS-V40. Test specimens were heated up to 1200 °C for 5 min to austenitize and cool down to test temperature at 1000 °C. Samples were held at the test temperature for 5 min to avoid temperature gradient. The first hit was applied, followed by varying interpass time (based on empirical equations) before the second hit. In both hits, strain was applied up to 0.3 strain at $1\,s^{-1}$ strain rate. To ensure a low friction interface and provide temperature uniformity, 0.1 mm graphite foil and 0.1 mm tantalum foil were used at both contact surfaces between UCT samples and anvils.[22]

3. Results

3.1. Effective Strain Distribution After Deformation

Figure 2a shows the predicted strain distribution in the UCT sample for 0.3 macroscopic deformations and at $1\,s^{-1}$ strain rate. A strain distribution can be seen from the center to the top/bottom surface due to the friction between the sample and anvils. The edges experience the largest strain (0.56) compared with other parts of the sample. The range of strain in the central part of the sample shown as a circular section in Figure 2b is 0.38–0.44, exceeding the applied macroscopic strain. The material that experiences ±10% of the applied macroscopic strain is in the region between the center and sides of the sample, which is difficult to section for microstructural analysis; however, this accounts for ≈60% of the sample volume shown in Figure 2c. Figure 2d shows the predicted strain distribution in the PSCT1 sample for applied 0.3 macroscopic strain. Shear bands are formed from the area of the sample in contact with the corner of the anvils and, these meet at the central area of the sample. The strain in the central area (0.44–0.5) is much higher than the applied 0.3 macroscopic strain, shown in Figure 2e. The material near the sample surfaces, away from the anvil edges, experiences a low strain (0.15–0.25), occupying a significant percentage of the deformed sample volume, Figure 2f, therefore the volume experiencing ±10% applied macroscopic strain only accounts for 13% of the deformed region. It can be observed that both UCT and PSCT1 sample geometries suffer from nonuniform strain distributions, and the strain level in the central area is much higher than the applied macroscopic strain.[17,22] Therefore, these samples are not appropriate to use for microstructure analysis where a large area of known (ideally equal to the applied macroscopic strain) uniform strain is required. In PSCT 2, the width of the anvils has been increased to 20 mm to minimize the effect of the shear strains seen in PSCT1. Figure 2g,h shows the strain distribution in the PSCT2 sample and throughout the cross section for the applied 0.3 macroscopic strain. The uniformity of strain in the PSCT2 sample increased significantly compared with PSCT1. Therefore, the PSCT2 sample is comparatively more favorable for microstructure analysis.[22] The volume of the deformed sample region that experiences ±10% of the applied 0.3 strain is ≈ 60%, shown in Figure 2i.

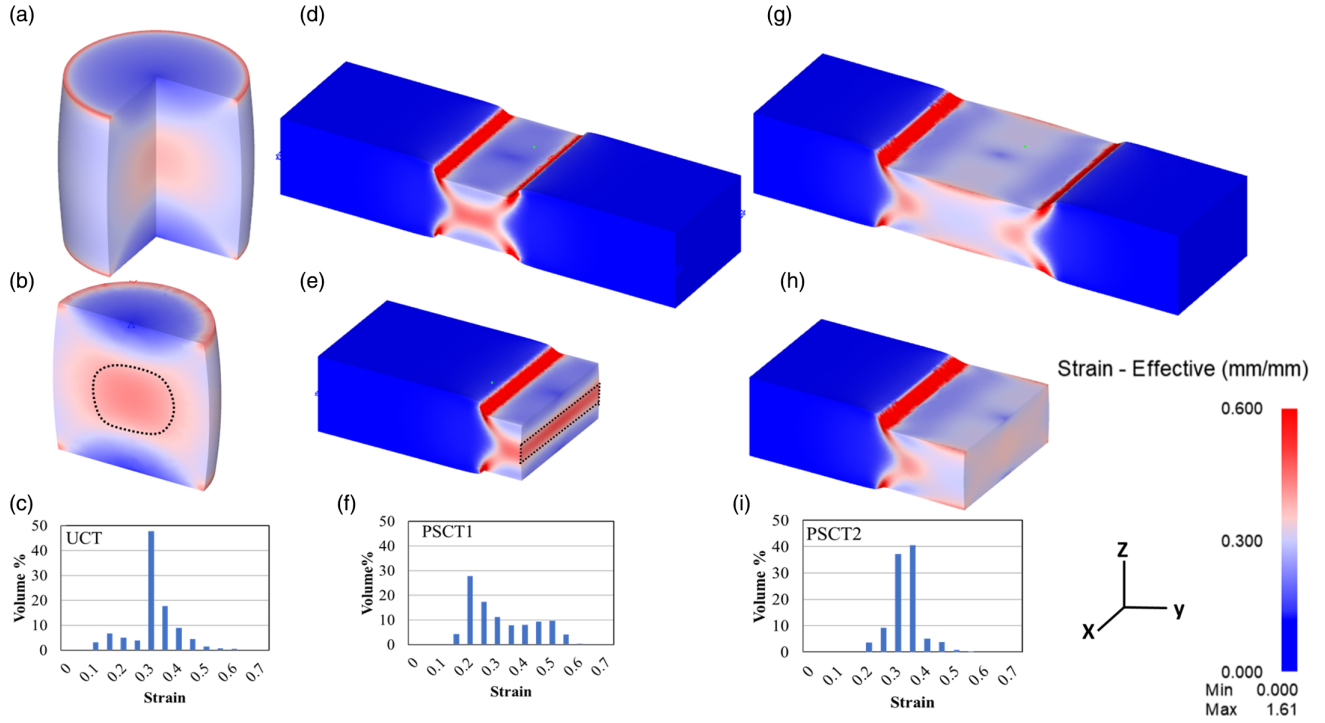

Figure 2. Strain distribution in a) UCT sample, d) PSCT1 sample, and g) PSCT2 sample after an applied macroscopic strain of 0.3 and histogram of vol% of the deformed region experiencing the different strain values for c) UCT sample, f) PSCT1 sample, and i) PSCT2 sample. The dashed areas in (b) and (e) represent the central area in the UCT and PSCT1 samples with a relatively high strain and the PSCT2 sample in (h) shows relatively uniform strain throughout the *x*–*z* plane.

3.2. Double Hit Test

The effect of UCT, standard PSCT, and modified PSCT samples geometries on strain uniformity and its subsequent effect on the prediction of softening fraction from double hit flow stress, simulations were performed for double hit tests. The interpass time was varied based on the applied macroscopic strain and material softening kinetics (empirical equations) to achieve 0–99% softening volume percentages.

Figure 3a shows the predicted flow stress curves for the double hit tests for all three geometries when no softening occurs. PSCT1 sample shows overall higher flow stress as this sample experiences higher strain volume results and more work hardening in the system causes higher flow stress compared with UCT and PSCT2 samples. Simulations were also carried out with an interpass time to achieve 99% softening based on empirical equations for 0.3 applied strain which is shown in Figure 3b. As there is strain inhomogeneity in the samples, full softening will not

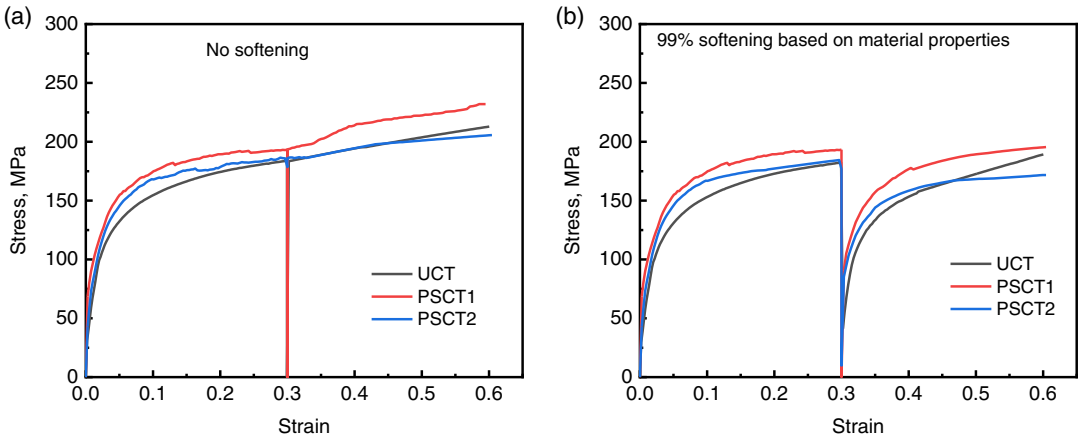

Figure 3. Flow stress of double hits test for a) no softening condition and b) 99% softening based on empirical equations.

complete in the low-strain regions. The predicted softening volume percentages from the flow stress curves, using Equation (1), are 87%, 77%, and 90% for UCT, PSCT1, and PSCT2, respectively. PSCT1 showed the greatest discrepancy with the large low-strain region at the top and bottom of the sample in contact with the anvils (Figure 2a,b) having a large effect on the outcome due to the high dependency of strain on the localized softening kinetics (fourth power as shown in Equation (2)). **Figure 4** shows the model outputs for the central section in the *X*-axis of the samples for the predicted strain and softened fraction for the 99% softening condition. The unsoftened regions at the sample surfaces due to the dead zones can be seen. The strain range in the dead zone is 0.06–0.25, which is much lower than the applied strain (0.3) and therefore, little/no softening is observed in this area even after the interpass time where 99% softening at 0.3 strain is predicted, while the central region of the sample is fully softened. The percentage of softening determined from the double hit flow stress data is higher for both the UCT and PSCT2 samples than the PSCT1 and closer to the expected behavior for the material; however, microstructure analysis (for grain size analysis) taken from a section through the center of the sample will be less accurate for the UCT sample than the PSCT2 sample because of the higher strain (0.38–0.44) in this region as recrystallised grain size is affected by the strain.[16,25] The PSCT2 sample shows uniform strain close to the applied macroscopic strain (0.27–0.33) up to ±5 mm from the center of the *Z*–*X* plane providing large volume for grain size analysis.

Figure 5 shows the predicted flow stress curves for the three sample geometries for the different interpass times (determined to produce 0%, 25%, 50%, 75%, and 99% softening for 0.3 strain) obtained from FEM models. As the interpass time increases, the softening volume percentage increases, and the flow stress in the second hit decreases. Figure 5a shows that the flow stress curves for the double hit tests for UCT, based on Equation (1), are 0%, 23%, 42%, 70%, and 87%, respectively. A similar pattern of flow stress is observed for the PSCT2 sample, shown in Figure 5c, where the predicted softening volume percentages are 0%, 27%, 49%, 71%, and 90%. For the PSCT1 sample geometry, the flow stress curves gave much higher softening volume percentages of 0%, 55%, 63%, 67%, and 77%, showing a significantly larger fraction softening in the early stages but completing with a much-reduced total softened fraction. A summary of the predicted softening volumes from the double hit flow stress curves for the different conditions is shown in **Table 2**.

4. Validation of the Model

To validate the model, UCT, PSCT1, and PSCT2 samples for four different interpass times to achieve softening conditions 25%, 50%, 75%, and 99% based on empirical equations were tested in the Gleeble simulator to produce double hit flow stress curves. The double hit flow stress curve obtained from UCT, PSCT1, and PSCT2 for all softening conditions is given in **Figure 6**. During

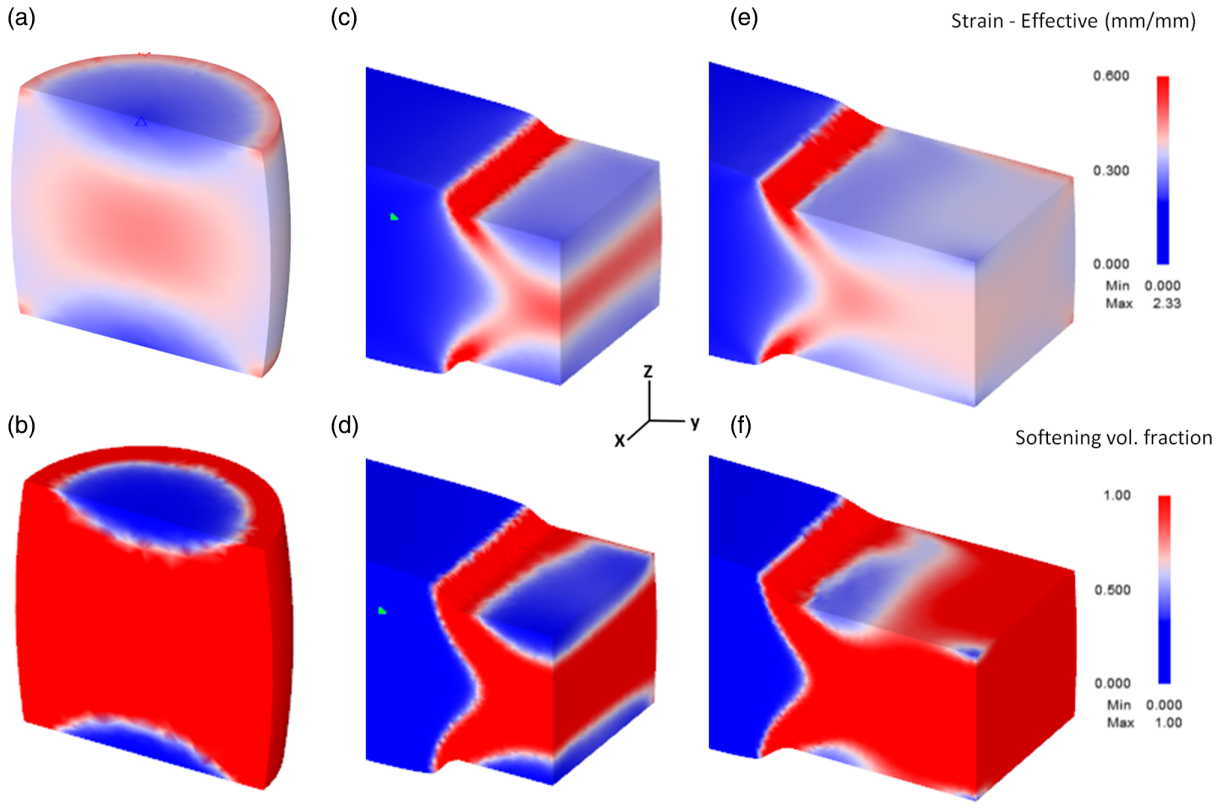

Figure 4. a) Strain and b) softening fraction for the UCT sample; c) strain and d) softening fraction for the PSCT1 sample; e) strain and f) softening fraction for the PSCT2 sample. All samples were modeled for the 99% softening condition based on the empirical equations (at 0.3 strain) and macroscopic applied 0.3 strain.

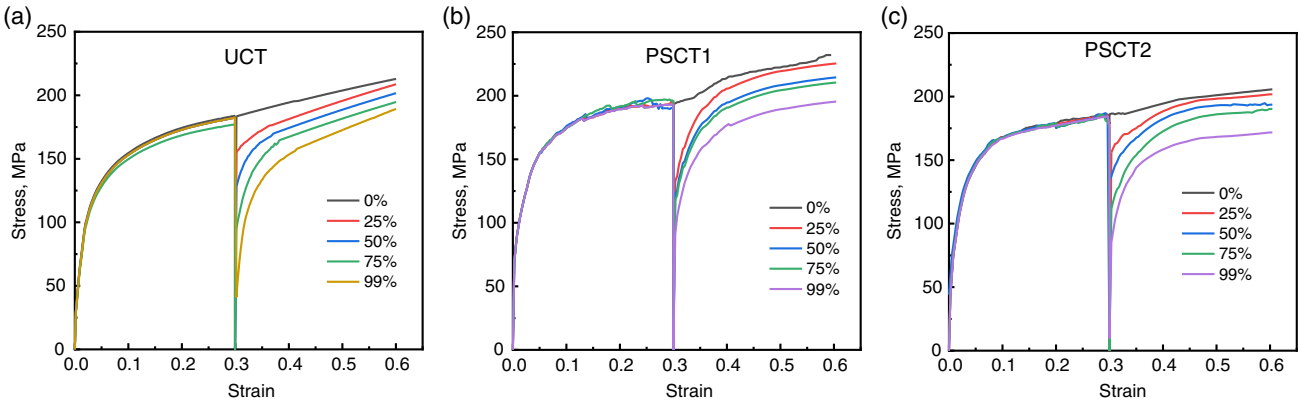

Figure 5. Predicted flow stress curves for different interpass times to achieve softening conditions 0%, 25%, 50%, 75%, and 99% based on empirical equations for a) UCT, b) PSCT1, and c) PSCT2.

the first deformation up to 0.3 strain, strain hardening occurs due to an increasing dislocation density in the steel. From literatures, it is observed that 0.3 strain is used to analyze static softening for C–Mn steel; therefore, no dynamic recovery or softening is expected for the applied strain of 0.3.[10,23,26] The flow stresses in the Figure 6 show no softening at the first hit up to 0.3 strain which additionally shows that no dynamic softening occurs during deformation. During the interpass time, recovery and nucleation of new strain-free recrystallizing grains occur at the grain boundary. For partial softening, not all the strained grains will soften, with grains with high dislocation density (i.e., smaller grains and those crystallographically favorably oriented for deformation—high Taylors factor) preferentially recrystallizing.[27,28] The second deformation curve shows the softening behavior of the material due to softening. The softening percentage was calculated using Equation (1). The calculated softening percentages for the 0%, 25%, 50%, 75%, and 99% conditions (based on empirical equations) for all samples are summarized in **Table 3**.

For 0% softening fraction condition, almost no softening was observed for all samples though PSCT1 was having high strain at the center. It could happen as both deformations occurred in less than 0.15 s at 1000 °C. The measured softening fractions for both PSCT2 and UCT show reasonably good agreement with the

Table 2. Summary of predicted softening fraction volume of UCT, PSCT1, and PSCT2.

Softening fraction value using empirical equations	Softening volume fraction from flow stress curves (modelling)		
	UCT	PSCT1	PSCT2
0	0	0	0
25	23	55	27
50	42	63	49
75	70	67	71
99	87	77	90

Table 3. Calculated softening percentage based on the Gleeble double hit flow stress curves compared with the predicted percentages based on the material behaviour at 0.3 strain.

Softening fraction value using empirical equations	Softening volume fraction (Experiments)		
	UCT	PSCT1	PSCT2
0	0	0	0
25	22	54	33
50	46	60	56
75	69	65	77
99	83	85	89

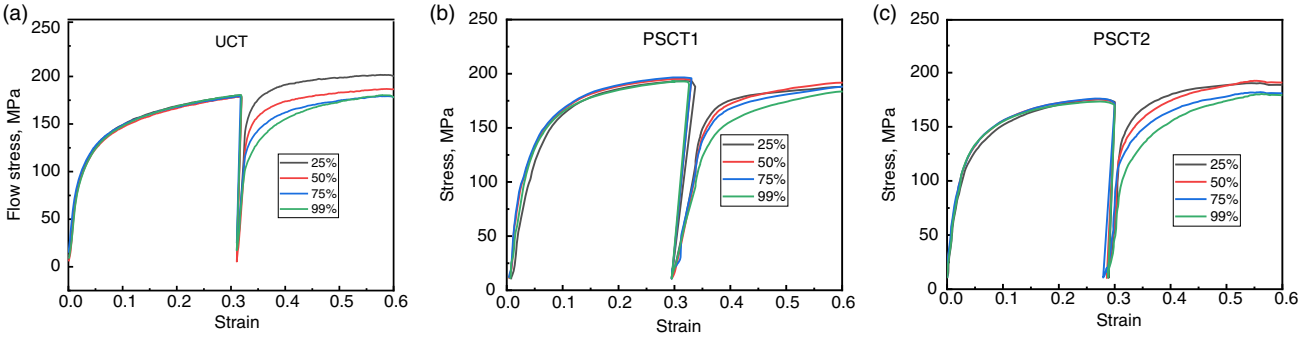

Figure 6. True stress versus true strain curve of PSCT2 sample for 50% softening condition at 1000 °C, at strain rate 1 s^{-1} for a) UCT, b) PSCT1, and c) PSCT2.

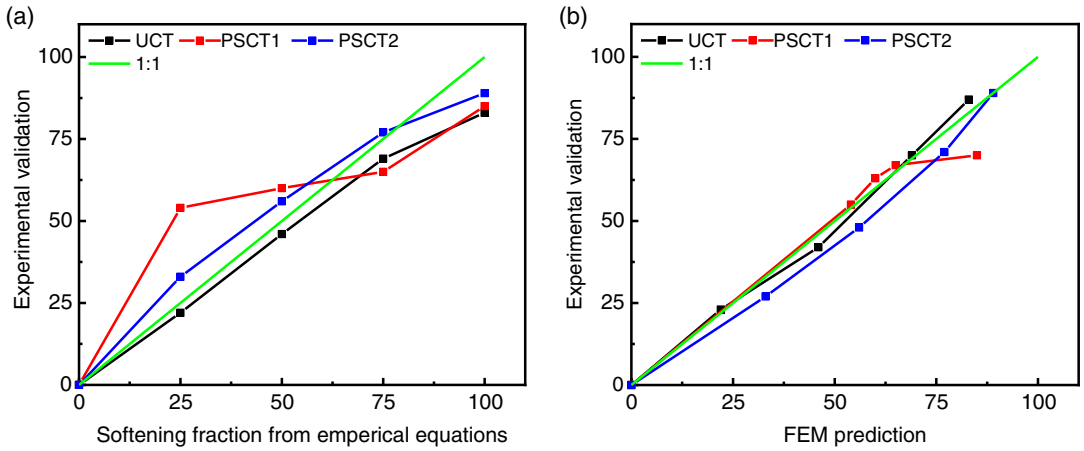

Figure 7. a) Comparison between softening fraction volume percentage from experiment and softening volume fraction based on the material softening kinetics and macroscopic strain and b) comparison between experimental and modeling results.

applied softening fraction volume from empirical equations. However, the measured softening fraction volume for PSCT1 is significantly higher than the applied 25% and 50% softening volume fraction and lower than 75% applied material conditions.

The empirical equations were used to calculate interpass time between double hit to achieve 0%, 25%, 50%, 75%, and 99% static softening fractions for a specific temperature (1000 °C) and macroscopically uniform strain (0.3). The calculated interpass times for specific softening fraction were used during Gleeble and FEM double hit tests and softening fraction was calculated from double hit flow stress. Then the measured softening fractions from Gleeble flow stress of different geometries were compared with the specific softening fractions from the empirical equations to compare the accuracy. A comparison between the softening volume percentages determined from the double hit flow stress curves from the experiments of different geometries and softening volume from empirical equations is shown in **Figure 7**a. Figure 7b shows the comparison between the experimental softening fraction and predicted softening fraction from modeling results. At the 25% softened condition based on empirical equations, the model double hit test produces 55% softening volume for the PSCT1 sample and 54% was obtained from the experiment (Figure 7b). There is good agreement between the model and experimental results. However, there is a large difference in the expected behavior due to the material response at 0.3 strain. As discussed above, this reflects the high volume of material at the sample center in the PSCT1 sample experiencing strains much higher than the applied 0.3 strain (i.e., ≈40% volume has a strain >0.3) and the strong dependency of localized softening on localized strain; therefore, high softening percentage in the center region was observed. While the regions with lower strain (<0.3) will show less softening, the nonlinear strain dependence means that the high-strain region has a greater effect on the flow stress. When the material softening percentage is high (99%), all volumes with strain above 0.3 will soften but as there are regions with lower strain (Figure 4), then the flow stress data will show a lower softening percentage. Overall, the experimental results for the PSCT1 sample geometry show good agreement with the simulation results. This indicates that the PSCT1 sample geometry is not ideal for calculating softening kinetics/predicting coefficient of the empirical equation for softening using double hit test.

However, for the PSCT2 and UCT sample geometries, a good agreement between experimental and model results is obtained, and these results agree reasonably well with the expected softening fraction from empirical equation. For 25% material input condition, UCT sample produces 23% and 22% softening fraction from the double hit flow stress of modeling and experiments, respectively, and the PSCT2 sample produces 27% and 33% softening volume percentage for modeling and experiments respectively. These samples show their capability to produce a more accurate softening fraction volume compared to PSCT1.

It is important to note that these simulations have not taken the practical variability seen in these tests into consideration, with the UCT being known to show thermal gradients along its length[18,29] as well as variability in friction coefficients due to anvil wear and choice of lubricant.[30–32] PSCT can be much less sensitive to these variables depending on the experimental setup (such as in a HDS-V40 Gleeble where the hot portion of the sample is not in contact with the anvils prior to deformation).[31] Any variations in temperature/friction will increase other errors associated with the double hit method.

5. Conclusion

The effect of sample geometries on the uniformity of the strain distribution in the sample and its effect on the calculation of softening volume fraction from double hit deformation tests has been investigated using DEFORM modeling software. A user-defined routine was developed and coupled with DEFOM to run double hit tests. The localized softening fraction was calculated from localized strain, and the strain value was replaced to zero when the softening fraction reached 85% during the interpass time using user routine.

Three sample geometries have been considered, a standard uniaxial compression test sample (UCT), a standard plane strain compression test sample (PSCT1), and a modified plane strain

compression test sample designed to provide a more uniform strain distribution (PSCT2) using a wider anvil. The following conclusions can be made. 1) UCT and PSCT2 both samples showed good agreement between empirical and DEFORM simulations for double hit tests carried out between 0% and 99% softening, with around 10% underprediction being seen at 99%. However, PSCT1 showed a greater disagreement with discrepancies of up to 30% being seen; 2) The PSCT1 showed only 13% of its strain falling with the ±10% of the macroscopically applied strain (0.3) as opposed to the ≈60% of the UCT and PSCT2 samples; 3) Experimental verification carried out showed excellent agreement with the DEFORM simulations with maximum 8% discrepancy.

This is suggested that both UCT and PSCT2 samples are appropriate for double hit tests for the purpose of determining the softening fraction volume. PSCT1 however showed good agreement only when coupled with FEM and as such has limited appropriateness for the determination of the softening fraction volume.

Acknowledgements

The authors would like to thank the High Value Manufacturing Catapult at WMG for their ongoing support for research and Jenee Rolls for UCT samples preparation.

Conflict of Interest

The authors declare no conflict of interest.

Data Availability Statement

The data that support the findings of this study are available from the corresponding author upon reasonable request.

Keywords

double hit tests, plane strain tests, static softening, uniaxial compression tests

Received: February 28, 2022
Revised: July 22, 2022
Published online:

[1] B. López, J. M. Rodriguez-Ibabe, *Recrystallisation and Grain Growth in Hot Working of Steels*, Woodhead Publishing Limited, CEIT and Tecnun (University of Navarra), Spain **2012**, https://doi.org/10.1533/9780857096340.1.67.
[2] T. Inoue, H. Qiu, R. Ueji, *Metals* **2020**, *10*, 91.
[3] C. X. Yue, L. W. Zhang, J. H. Ruan, H. J. Gao, *Appl. Math. Modell.* **2010**, *34*, 2644.
[4] S. Li, Z. Eliniyaz, F. Sun, Y. Shen, L. Zhang, A. Shan, *Mater. Sci. Eng., A* **2013**, *559*, 882.
[5] Gleeble, https://www.gleeble.com/, n.d. (accessed: February 2022).
[6] ServoTest, https://www.servotestsystems.com/ (accessed: August 2022).
[7] D.R. Forrest, M.F. Sinfield, Numerical Simulation of Gleeble Torsion Testing of HSLA-65 Steel, **2008** https://apps.dtic.mil/sti/citations/ADA494364.
[8] R. Tucceri, *Surf. Sci. Rep.* **2004**, *56*, 85.
[9] T. J. Ballard, J. G. Speer, K. O. Findley, E. De Moor, *Sci. Rep.* **2021**, *11*.
[10] S. Bao, G. Zhao, C. Yu, Q. Chang, C. Ye, X. Mao, *Appl. Math. Modell.* **2011**, *35*, 3268.
[11] X. Wang, K. Chandrashekhara, M. F. Buchely, S. Lekakh, D. C. Van Aken, R. J. O'Malley, G. W. Ridenour, E. Scheid, *J. Manuf. Process.* **2020**, *52*, 281.
[12] X. Sun, M. Zhang, Y. Wang, J. Liu, *Steel Res. Int.* **2021**, *92*, 2000443.
[13] A. Grajcar, P. Skrzypczyk, R. Kuziak, K. Gołombek, *Steel Res. Int.* **2014**, *85*, 1058.
[14] A. Najafizadeh, J. J. Jonas, G. R. Stewart, E. I. Poliak, *Metall. Mater. Trans. A* **2006**, *37*, 1899.
[15] P. Kalinowski, C. L. Davis, M. Strangwood, https://etheses.bham.ac.uk/id/eprint/7921/ (accessed: August 2022).
[16] A. Kundu, C. L. Davis, M. Strangwood, *Metall. Mater. Trans. A* **2010**, *41*, 994.
[17] A. P. Carvalho, L. M. Reis, R. P. R. P. Pinheiro, P. H. R. Pereira, T. G. Langdon, R. B. Figueiredo, *Metals* **2022**, *12*, 125.
[18] A. Chamanfar, H. S. Valberg, B. Templin, J. E. Plumeri, W. Z. Misiolek, *Materialia* **2019**, *6*, 100319.
[19] X. Wang, H. Li, K. Chandrashekhara, S. A. Rummel, S. Lekakh, D. C. Van Aken, R. J. O'Malley, *J. Mater. Process. Technol.* **2017**, *243*, 465.
[20] Y. Xu, C. Chen, X. Zhang, H. Dai, J. Jia, Z. Bai, *Mater. Charact.* **2018**, *145*, 39.
[21] M. S. Mirza, C. M. Sellars, *Mater. Sci. Technol.* **2001**, *17*, 1142.
[22] C. Slater, N. Tamanna, C. Davis, *Results Mater.* **2021**, *11*, 100218.
[23] C. M. Sellars, *Mater. Sci. Technol.* **1990**, *6*, 1072.
[24] D. J. Cha, D. K. Kim, J. R. Cho, W. B. Bae, *Int. J. Precis. Eng. Manuf.* **2011**, *12*, 331.
[25] C. Slater, A. Mandal, C. Davis, *Metall. Mater. Trans. B* **2019**, *50*, 1627.
[26] S. Gardner, W. Li, M. Coleman, R. Johnston, *Mater. Sci. Eng., A* **2016**, *668*, 263.
[27] K. H. Chia, K. Jung, H. Conrad, *Mater. Sci. Eng., A* **2005**, *409*, 32.
[28] A. Kundu, D. P. Field, *Mater. Sci. Eng., A* **2016**, *667*, 435.
[29] G. Venet, C. Baudouin, C. Pondaven, R. Bigot, T. Balan, *Int. J. Mater. Form.* **2021**, *14*, 929.
[30] C. J. Bennett, S. B. Leen, E. J. Williams, P. H. Shipway, T. H. Hyde, *Comput. Mater. Sci.* **2010**, *50*, 125.
[31] D. Szeliga, J. Gawad, M. Pietrzyk, *Comput. Methods Appl. Mech. Eng.* **2006**, *195*, 6778.
[32] X. G. Fan, Y. D. Dong, H. Yang, P. F. Gao, M. Zhan, *J. Mater. Process. Technol.* **2017**, *243*, 282.